The suppression of phonon induced noise in niobium superconducting tunnel junction x-ray detectors

A. Poelaert, A. Peacock, N. Rando, P. Verhoeve, and P. Videler
Astrophysics Division, Space Science Department, European Space Agency, ESTEC, Noordwijk, The Netherlands

(Received 20 February 1995; accepted for publication 1 November 1995)

An investigation into the phonon contamination of x-ray sensitive superconducting tunnel junctions arising from the x-ray photoabsorption in various substrates has been conducted. Results are presented on the design of a superconducting tunnel junction (STJ) which substantially reduces or even eliminates phonon induced noise from the substrate. Such noise is the predominant feature in x-ray spectra from junctions due to the bulk of the photons being absorbed in the substrate rather than in the thin superconducting film. The design involves the choice of a suitable buffer sandwich between the substrate and the STJ. Such a buffer would appear not only to attenuate the phonons created in the x-ray photoabsorption in the substrate but also to scatter the phonons inelastically, introducing a frequency down-conversion. Such a process ensures that few phonons of energy sufficient to break Cooper pairs in the superconducting film of the STJ enter the junction. © *1996 American Institute of Physics.* [S0021-8979(96)08803-3]

I. INTRODUCTION

Superconducting tunnelling junctions (STJs) are under very active development as x-ray detectors by a number of groups.[1–5] Most of this development activity is based on niobium devices. The STJ offers distinct advantages over both semiconductor detectors or supercooled bolometers. In the former case the energy resolution is about 15 times worse than that predicted theoretically for an STJ,[1] i.e., below 10 eV for photon energies of around 6 keV. In the latter case the operating temperature is far lower, i.e., about 50 mK (Ref. 6) compared to 1 K for a Nb based device. Even with this rather intense effort to develop such STJ devices as practical spectrometers major problems remain unsolved. Of these the most important is the achieved energy resolution which is still over an order of magnitude worse than predicted.[2,5,7]

Other issues affecting the practical application of the STJ include the very low x-ray absorption efficiency, which is limited by the thin films necessary to achieve even the present relatively poor performance. The charge collected from the device is, to a first approximation, inversely proportional to the confinement time in the film. This is considered to depend not only on the properties of the barrier but also on the film grain structure and film thickness.[1] Hence the presently employed thin films are too transparent to x-ray photons, which therefore are absorbed in the substrate directly below the STJ. For example a typical Nb based STJ with film thicknesses of 0.14 μm is expected to absorb 4% of 6 keV x rays illuminating directly the device, the other 96% being absorbed in the substrate. Such substrate events are not simply lost from the system but are a source of phonon noise.[1] This phonon source can be detected by the junction either as discrete low energy events or as a delayed source of noise which degrades the spectra of events absorbed directly in the Nb film. In this paper we investigate experimentally the response of different types of substrates and buffer layers with a view to suppressing or eliminating this source of spectral contamination.

II. EXPERIMENTAL CONFIGURATION

Several substrates were selected with a view to depositing STJs on them. They are listed in Table I, together with their important properties. The evaluation of the phonon transmission coefficients in Table I assumed an isotropic phonon distribution with a Debye energy spectrum. This excess nonequilibrium phonon population is assumed to arise as a direct result of the absorption by the substrate of 6 keV x rays. The calculation of these coefficients follows similar work using an acoustic mismatch model[8,10,11] and is described in Appendix A.

On most of the samples, one or two buffer layers were deposited before the STJ. The various configurations studied are listed in Tables II and III.

Eight junctions were deposited on each substrate (12×12 μm^2, 20×20 μm^2, and 50×50 μm^2), forming a single chip. A schematic cross-section of a typical junction is shown in Figure 1. The base film is made of 500 Å polycrystalline Nb + 50 Å polycrystalline Al. The barrier was produced through the oxidation of this Al layer and has a resistivity of $\sim 2.5\times10^{-6}$ $\Omega\,cm^2$. The top electrode consists of 850 Å of Nb, also polycrystalline. Such thin films are very well suited for the observation of substrate events.

The chip has been placed in a vacuum environment and clamped to a cold finger, cooled via a pumped ^{4}He cryostat. A magnetic field was applied by a superconductor magnet, in order to suppress the dc Josephson current. An ^{55}Fe source was included in the vacuum environment, about 3 mm away from the junction. The current pulses from the detectors were fed into a charge sensitive preamplifier and a shaping stage, operating at room temperature, and optically coupled to a PC. A constant threshold was set up so as to suppress spurious signals, noisy events at low signal, generated or picked up by the electronics itself.

 0021-8979/96/79(5)/2574/6/$10.00

TABLE I. Summary of basic substrate parameters: ρ is the material density in grams/cm^3; c_l and c_t are the phonon velocities in 10^5 cm/s, for L and T modes, respectively (see Ref. 8); Ω_d is the Debye energy in meV (see Ref. 8); A is the anisotropy factor, defined by the elastic constants: $A=2c_{44}/(c_{11}-c_{12})$ (see Ref. 8) - Note A=1 corresponds to an isotropic material; δ_x is the 1/*e* absorption depth for 6 keV x-rays in μm (see Ref. 9); T_l and T_t are the phonon transmission coefficients for L and T modes at the interface from the substrate to niobium film (Appendix A).

Substrate	ρ (g/cm^3)	c_1 (10^5 cm/s)	c_t (10^5 cm/s)	Ω_d (meV)	A	δ_x (μm)	T_1	T_t
Sapphire	3.99	10.90	6.45	90	1.37	37	0.93	0.84
Silicon	2.33	8.98	5.34	56	1.57	29	0.93	0.95
Quartz	2.66	6.09	4.09	49	1.44	49	0.81	0.94
Am quartz	2.64	5.79	3.75	48	1.00	49	0.82	0.94

III. JUNCTIONS DEPOSITED DIRECTLY ON A SUBSTRATE OR ON A THIN BUFFER LAYER

The configurations corresponding to simple substrates or substrates with a thin buffer layer between the substrate and the STJ are listed in Table II. As an example, Figure 2 illustrates the charge spectrum recorded from a junction deposited on a sapphire substrate, corresponding to configuration 2 of Table II. This spectrum contains 2 main types of events:

(1) high charge events from the junction and the leads: detection of the energy from a photon absorbed directly in the junction or in a lead;

(2) low charge events from the substrate: a photon absorbed in the substrate is down-converted into phonons which can propagate towards the junction; once there, they are still energetic enough to be detected.[1,14]

The detection of events via phonon propagation in the substrate has 2 main consequences on the signal. First, the amplitude of the signal is much lower, due to a non-negligible fraction of the phonons which, either miss the junction, or are reflected at the substrate-junction interface, or reach the base film after too many frequency down-conversions to be still able to break Cooper pairs in the junction. Second, the rise time of the signal of substrate events is much more spread around a higher average value than for the junction events. The scatter plot of charge against rise time shown in Figure 3 is a clear illustration of this phenomenon. In all configurations listed in Table II, the maximum charge output of the events having a large rise time distribution is about 25% of the maximum charge output from junction events. This value has been fixed as a reference for the separation between substrate and junction events, in all configurations. One exception to this approach was made (configuration 3 of Table III), for reasons explained later in the paper.

To measure the efficiency of substrate and buffer layers in the suppression of phonon noise, a parameter which is independent of the junction should be used. The count rate of substrate events is sensitive to small differences between various junctions; the ratio between the number of substrate events (N_S) and the total number of detected events (N_T) is a more appropriate parameter, since both N_S and N_T will be dependent on the junction properties in the same way. Here, we introduce the 'efficiency ratio' $\eta=1-(N_S/N_T)$. The closer is η to 1, the more efficient are the substrate and buffer layers in suppressing phonon noise.

Table II summarizes the experimentally measured efficiency ratio's η for different substrates in identical experimental conditions. Note that in the very efficient configuration 5 (amorphous quartz), the very small number of

TABLE II. Results summary from various substrates: The operating temperature was 1.2 K; the buffer layers are deposited between the substrate and the bottom Nb film of the STJ; t_{layer} is the thickness of these layers; λ_{sub} (see Refs. 12,13) is the mean free path for boundary scattering in the substrate for phonons with an energy equal to $2\,\Delta_{Nb}$ (equivalent to an angular frequency ω of 4.5 THz); the mean free path in amorphous quartz includes the interaction with fractions.

Configuration	Substrate	Buffer layers	t_{layer} (Å)	λ_{sub} (μm)	T_l	T_t	η
1	Sapphire	none		2000	0.93	0.84	0.048
2	Sapphire	AlO_x	50	2000	0.96	0.90	0.03
3	Silicon	SiO_2/AlO_x	10/33	410	0.53	0.60	0.053
4	Quartz	AlO_x	33		0.20	0.27	0.09
5	Am quartz	AlO_x	33	0.024	0.17	0.21	$\sim$0.75

TABLE III. Results summary from buffered substrates: The columns titled SiO_2 and AlO_x refer to the thicknesses of buffer layers made from such materials; *Abs* is the expected absorption of phonons with an energy $2\Delta_{Nb}$ which cross the buffer layers, without modification due to the transmission coefficients at the interfaces; *Att* combines the absorption and the transmittivity.

Configuration	Substrate	SiO_2 (Å)	AlO_x (Å)	T_l	T_t	*Abs* (%)	*Att* (%)	η
1	Sapphire	0	2000	0.96	0.90	68	70.5	~ 0.81
2	Silicon	1000	1000	0.53	0.60	99	99.4	~ 0.84
3	Silicon	1770	260	0.52	0.60	100	100	1

substrate events makes it rather difficult to determine the limit between substrate and junction events. The 25% threshold discussed previously was maintained, but however we cannot be sure that some junction or lead events were not also included in the determination of N_S.

The calculated mean phonon transmission coefficients T_l and T_t (for L & T modes, respectively) from the substrate to the niobium are also listed in Tables II and III. They include not only the presence of buffer layers but also the various critical angles that can arise (see Appendix A).

Analysis of the efficiency ratio's from Table II indicates values about 15 times lower for the various crystalline substrates as compared to that of the amorphous quartz. Obviously, the transmission coefficients for amorphous quartz (Table II) for the substrate–buffer–Niobium interface cannot account for the dramatic attenuation of the phonon flux reaching the niobium junction compared to single crystal quartz. The amorphous quartz must itself absorb a significant fraction of the phonons produced as a result of an x-ray photoabsorption. It is clear that significant attenuation would occur in amorphous quartz compared to single crystal quartz as a result of its very small phonon mean free path λ_{sub} of order 240 Å. The small differences in η for the crystalline substrates can be easily accounted for by the transmission coefficients T_l and T_t: the lower the phonon transmission through the interface, the higher η. Basically, these differences in phonon transmission are due to the values of the critical angles, which are 36 and 46 degrees (for L and T modes respectively) from quartz to AlO_x and which do not exist from sapphire to AlO_x and from AlO_x to Nb.

IV. JUNCTIONS DEPOSITED ON THICK BUFFER LAYERS

To examine the role of amorphous materials in attenuating the substrate phonon flux a range of buffer layers was investigated. As a key example, Figure 4(a) illustrates a charge spectrum while 4(b) shows the equivalent charge vs rise time scatter plot for configuration 3 in Table III. Very few events were detected below 25% of the maximum charge output. Moreover, these residual events cannot be attributed to phonon noise. Indeed, this low charge peak is actually restricted to a specific range of low charge outputs and is located at a charge value expected for the Si–K x-ray line. Fluorescence in the silicon substrate would appear to be responsible of this feature, rather than phonon contamination. Another argument which supports this interpretation is that the large rise time dispersion seen at low charge values in Figure 3 do not appear at all in Figure 4(b). This implies that η is very close to 1.

Table III also summarizes the measured values of η for other buffer layers, along with the total transmission coefficient for either L or T modes due to all the interfaces between the substrate and the Niobium film. This coefficient includes multiple reflections at any interface but not phonon attenuation due to the substrate or buffer material. In addition, Table III also provides the expected absorption (Abs) of 2Δ phonons through the various buffer layers without modification due to the transmission coefficients at the interfaces. This absorption is given by:

$$Abs = 100 \cdot e^{-\frac{t_{layer}}{\lambda}}\% \tag{1}$$

with t_{layer} the thickness of the layer and λ the phonon mean free path in such a layer. The mean free path λ is calculated in Appendix B for SiO_2 and AlO_x, giving 240 Å and 1760 Å, respectively. Note, λ_{AlO_x} was calculated based on a comparison with λ_{SiO_2}, since no experimental data are currently available. The column titled Att in Table III shows the total attenuation due to the combination of the two phenomena.

The values of η for configurations 2 and 3 of Table III are consistent with the values reported in Table II. In configuration 1 however η is far too large. As an example, the transmission coefficients in configuration 4 of Table II would give rise to an attenuation of about 70%, which is close to Att of the first configuration of Table III. This could be due to an overestimation of λ in AlO_x used to determine Abs. Essentially, the various hypotheses and approximations used in the model of Appendix B effectively only allow a rough estimate of λ_{AlO_x}. This could mean that λ_{AlO_x} is uncertain by about a factor of 2, leading to an attenuation of 90.6% instead of the 70.5% indicated in Table III.

It is clear however that SiO_2 is a far more efficient phonon absorber than AlO_x. The main role of AlO_x is to introduce a small critical angle for phonons incident from an SiO_2 layer, and thereby reflect most of the few remaining phonons. Any substrate therefore with a SiO_2 thickness of over 1100 Å will attenuate the phonon flux from the substrate by 2 orders of magnitude. In the case of the double buffer of 1760 Å SiO_2 and 260 Å AlO_x the phonon flux through this buffer is practically zero due totally to the thickness of the SiO_2 layer.

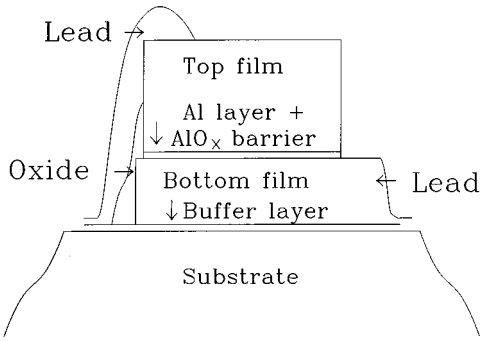

FIG. 1. A schematic cross section of Nb−Al−AlO_x−Nb junction deposited on sapphire, with a 50 Å AlO_x buffer layer. Note the aluminum is deposited on the Nb base film, and the barrier is formed through the oxidation of this layer.

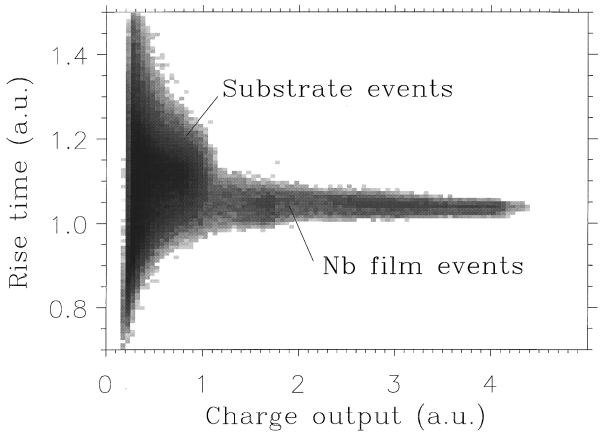

FIG. 3. The charge vs rise time scatter plot corresponding to the charge spectrum of Figure 2. The low charge output events are much more spread in rise time, around a higher average. These are the events absorbed in the substrate, while the others arise from the junction and the leads.

V. CONCLUSION

The ability to suppress the substrate induced phonon noise in STJs has been rather conclusively demonstrated. A double buffer layer of 1100 Å SiO_2 with a few tens Å AlO_x should effectively reduce the contamination to below 1%. The best substrate for intrinsically suppressing this noise source is amorphous quartz. A combination of amorphous quartz with a buffer layer of SiO_2 is the most effective combination of materials to ensure phonon noise free superconducting tunnel junctions.

APPENDIX A: THE PHONON TRANSMISSION AT AN INTERFACE

The total energy transmission coefficient as a result of the various interfaces has been evaluated using the work of Reference 11 and verified based on the work of References 8 and 10. In general the approach adopted here differs from Reference 8 by at most 10%.

Let us consider two semi infinite materials, defined by the indexes 1 and $n+1$, separated by $n-1$ layers (indexed 2 to n). The solution for the final transmission coefficient of a wave propagating in such a layered medium is well established. Such a wave may propagate in medium n and reach the $(n,n+1)$ interface with an incident angle θ_{n+1}. To evaluate the total energy transmission coefficient as a result of the propagation through all $n-1$ layers the incident wave pres-

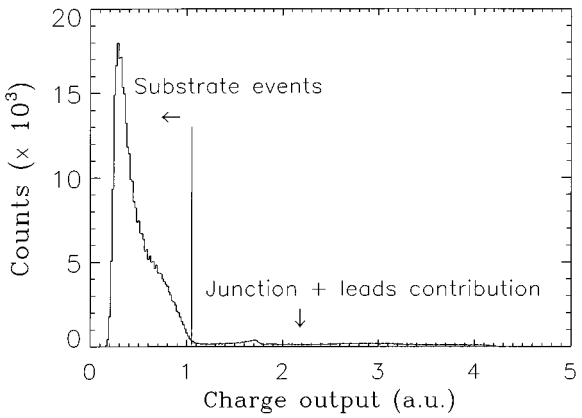

FIG. 2. Charge spectrum of the junction of Figure 1, illuminated with an ^{55}Fe source. The vertical line separates the substrate events (left peak) from the junction and leads contribution (to the right).

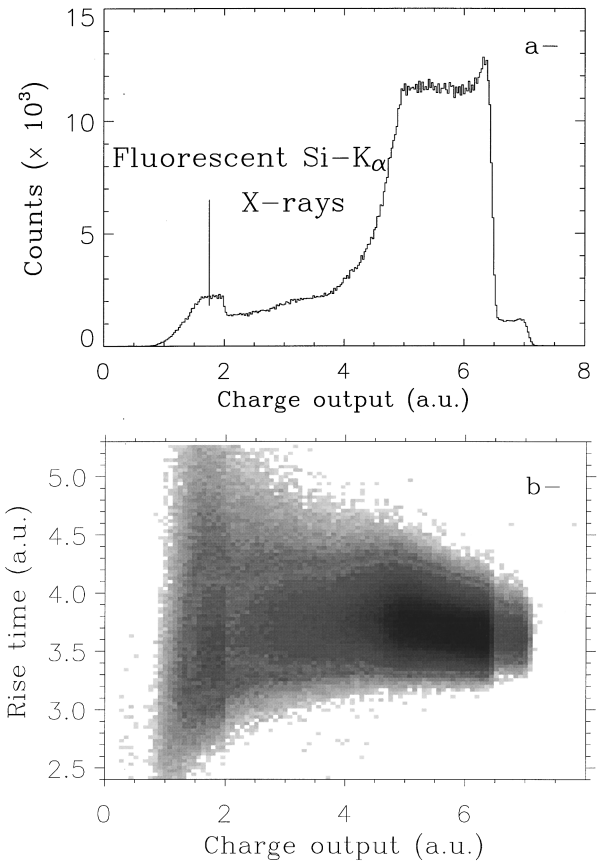

FIG. 4. (a) Charge spectrum from an ^{55}Fe source illuminating a STJ in configuration 3 of Table III. (b) The charge vs rise time scatter plot corresponding to (a).

sure must be determined. The pressure P_i of such a wave incident at time t and at a position *x,y,z,* can be written as:

$$P_i(x,y,z,t)=e^{-i[k_i(r-r_0)-\omega t]}, \tag{A1}$$

where k_i is the wave vector for the incident wave, r the position vector, r_0 the incident point and ω is the angular frequency. Note the z coordinate at the $(n,n+1)$ interface is simply z_n. The reflected wave pressure P_r can be written:

$$P_r(x,y,z,t)=R(\omega,\theta_{n+1})e^{-i[k_r(r-r_0)-\omega t]} \tag{A2}$$

Here k_r has the same modulus as k_i but a different propagation direction, $R(\omega,\theta_{n+1})$ is the pressure reflection coefficient. Naturally the transmitted wave for the case when $z_1=0$ is

$$P_t(x,y,z,t)=T_1(\omega,\theta_{n+1})e^{-i(k_t r-\omega t)}. \tag{A3}$$

Under the assumption that the boundary conditions of continuity of pressure and phonon velocities in the z direction exist at the interface, the reflection coefficient R can be written

$$R(\omega,\theta_{n+1})=\frac{Z_n'(\omega,\theta_{n+1})-Z_{n+1}(\theta_{n+1})}{Z_n'(\omega,\theta_{n+1})+Z_{n+1}(\theta_{n+1})} \tag{A4}$$

where:

(1) $Z_{n+1}(\theta_{n+1})$ is the wave impedance in medium $n+1$ defined by:

$$Z_{n+1}(\theta_{n+1})=\left.\frac{P_i}{\cos(\theta_{n+1})}\right|_{z=z_n}=\frac{\rho_{n+1}v_{n+1}}{\cos(\theta_{n+1})} \tag{A5}$$

with ρ_{n+1} being the density of material $n+1$ and v_{n+1} the phonon velocity.

(2) $Z_n'(\omega,\theta_{n+1})$ is the internal impedance of materials $1-n$ and can be derived from the recursive relation

$$Z_n'(\omega,\theta_{n+1})=\frac{Z_{n-1}'(\omega,\theta_{n+1})-iZ_n(\omega,\theta_{n+1})\tan(k_{nz}d_n)}{Z_n(\omega,\theta_{n+1})-iZ_{n-1}'(\omega,\theta_{n+1})\tan(k_{nz}d_n)}\times Z_n(\omega,\theta_{n+1}) \tag{A6}$$

where k_{nz} is the wave vector in the nth layer in the z direction and d_n is the thickness of this layer.

Assuming that no phonon absorption actually occurs in the various layers the energy transmission coefficient T can be written as:

$$T_1(\omega,\theta_{n+1})=\sqrt{1-|R(\omega,\theta_{n+1})|^2}. \tag{A7}$$

The transmission coefficient function of Equation (A7) can be further simplified assuming that all phonon energies are distributed according to a simple Debye spectrum and are propagated isotropically.

For such a Debye distribution we can write:

$$T(\theta_{n+1})=\frac{\int_0^{\omega_D}g(\omega)T_1(\omega,\theta_{n+1})d\omega}{\int_0^{\omega_D}g(\omega)d\omega} \tag{A8}$$

where $g(\omega)$ is the spectral density in medium n+1 and ω_D is the Debye energy in the same medium.

For an isotropic phonon propagation we can write:

$$T=2\int_0^{\frac{\pi}{2}}T(\theta_{n+1})\sin(\theta_{n+1})\cos(\theta_{n+1})d\theta_{n+1}. \tag{A9}$$

To illustrate the approach we take as an example a multilayer consisting of a silicon substrate with a 33 Å aluminum oxide layer followed by a niobium layer which would form part of the STJ. Only phonon angular frequencies ranging from 4.5 THz (3 meV = $2\Delta_{\mathrm{Nb}}$) to 84.5 THz (55.9 meV = ω_D^{Si}) need be considered in this example since lower frequency phonons cannot break Cooper pairs in the Niobium. A critical incident angle between the silicon and the first layer of AlO_x exists and can be derived based on the Snell-Descarte law:

$$\theta_c=\arcsin\left(\frac{v_{\mathrm{Si}}}{v_{\mathrm{AlO_x}}}\right)=60°. \tag{A10}$$

Here v is the longitudinal phonon velocity. Only phonons which reach the interface with an incident angle below the critical angle are considered in our computation. The acoustic impedance for each of the materials can be written:

$$Z_{\mathrm{Nb}}(\theta)=\frac{\rho_{\mathrm{Nb}}v_{\mathrm{Nb}}}{\sqrt{1-\left(\frac{v_{\mathrm{Nb}}}{v_{\mathrm{Si}}}\sin(\theta)\right)^2}} \tag{A11}$$

$$Z_{\mathrm{AlO_x}}(\theta)=\frac{\rho_{\mathrm{AlO_x}}v_{\mathrm{AlO_x}}}{\sqrt{1-\left(\frac{v_{\mathrm{AlO_x}}}{v_{\mathrm{Si}}}\sin(\theta)\right)^2}} \tag{A12}$$

$$Z_{\mathrm{Si}}(\theta)=\frac{\rho_{\mathrm{Si}}v_{\mathrm{Si}}}{\cos(\theta)} \tag{A13}$$

while the wave vectors are simply

$$k_{\mathrm{Nb}}(\omega_j)=\frac{\omega_j}{v_{\mathrm{Nb}}}, \tag{A14}$$

$$k_{\mathrm{AlO_x}}(\omega_j)=\frac{\omega_j}{v_{\mathrm{AlO_x}}}, \tag{A15}$$

$$k_{\mathrm{Si}}(\omega_j)=\frac{\omega_j}{v_{\mathrm{Si}}}. \tag{A16}$$

Based on Equations (A1)–(A8) discussed above and considering that $g(\omega)$ is proportional to ω^2 for a Debye spectrum, the total energy transmission coefficient can be simply derived as:

$$T(\theta)=\frac{\int_0^{\omega_D}\omega^2T(\omega,\theta)d\omega}{\int_0^{\omega_D}\omega^2d\omega}. \tag{A17}$$

Finally, we solve for T using Equation (A9).

APPENDIX B: THE PHONON MEAN FREE PATH IN AMORPHOUS MATERIALS

For low frequency systems ($f<f_c$ where f_c is a crossover frequency), the phonon mean free path in amorphous materials can be written:[15–17]

$$\lambda = \frac{\rho v^3}{\pi n_0 B^2 \omega} \coth\left(\frac{\hbar\omega}{2k_B T}\right) \tag{B1}$$

with ρ the material density; v the mean phonon velocity in this material; n_0 the density of TLS (Two Level Systems: see Refs. 15–17) per unit volume and energy interval; B the deformation potential constant; and ω the angular frequency $(2\pi f)$.

Hence, at very low temperatures (i.e., in the current situation), we can assume λ as a simple inverse function of the frequency f.

For higher frequency systems the mean free path λ is proportional to f^{-3}.[18,19] For SiO_2 the experimental function reported by Dietsche and Kinder[18]at high phonon frequencies was

$$\lambda_{SiO_2}(f) = 10^5 \text{ Å}\left(\frac{100 \text{ GHz}}{f}\right)^3. \tag{B2}$$

This cubic dependence includes the phonon-fracton interaction.[19] Since the mean free path is continuous with f, relations (B1) and (B2) must be identical at f_c, giving:

$$\lambda_{SiO_2}(f_c) = \frac{\rho_{SiO_2} v_{SiO_2}^3}{2\pi^2 n_{0_{SiO_2}} B_{SiO_2}^2 f_{c_{SiO_2}}} = 10^5 \text{ Å}\left(\frac{100 \text{ GHz}}{f_{c_{SiO_2}}}\right)^3 \tag{B3}$$

which implies

$$\lambda_{SiO_2}(f > f_c) = \frac{\rho_{SiO_2} v_{SiO_2}^3 f_{c_{SiO_2}}^2}{2\pi^2 n_{0_{SiO_2}} B_{SiO_2}^2} \times \frac{1}{f^3}. \tag{B4}$$

Based on this relation and on the correspondent one for AlO_x, we find:

$$\frac{\lambda_{SiO_2}}{\lambda_{AlO_x}} = \frac{\rho_{SiO_2}}{\rho_{AlO_x}} \left(\frac{v_{SiO_2}}{v_{AlO_x}}\right)^3 \left(\frac{B_{AlO_x}}{B_{SiO_2}}\right)^2 \frac{n_{0_{AlO_x}}}{n_{0_{SiO_2}}} \left(\frac{f_{c_{SiO_2}}}{f_{c_{AlO_x}}}\right)^2. \tag{B5}$$

Note, n_0 is generally considered to be proportional to the number of atoms per unit volume of the material divided by the Debye frequency, with a factor independent of material. Thus:

$$n_0 \propto \frac{N\rho}{M\omega_D} \tag{B6}$$

where N is the number of atoms per molecule and M the molecular weight.

For the purpose of this paper, we set $f_{c_{AlO_x}} = f_{c_{SiO_2}}$, although this assumption must be taken with some caution. Hence, Equations (20) and (23) give

$$\lambda_{SiO_2} = 240 \text{ Å}, \tag{B7}$$

$$\lambda_{AlO_x} = 1760 \text{ Å}. \tag{B8}$$

[1] N. Rando, A. Peacock, A. van Dordrecht, C. Foden, R. Engelhardt, B.G. Taylor, P. Gare, J. Lumley, and C. Pereira, Nucl. Instrum. Meth. Phys. Res. A **313**, 173 (1992).
[2] C.A. Mears, S.E. Labov, and A.T. Barfknecht, J. Low Temp. Phys. **93**, 561 (1993).
[3] P.A.J. de Korte, ESA Symposium on Photon Detectors for Space Instrumentation, ESA (1992), Vol. SP-356, p. 41.
[4] M. Kurakado, Nucl. Instrum. Meth. **196**, 275 (1982).
[5] P. Verhoeve, N. Rando, P. Videler, A. Peacock, A. van Dordrecht, D.J. Goldie, J.M. Lumley, J. Howlett, M. Wallis, and R. Venn, SPIE July, 2283 (1994).
[6] S.H. Moseley, M. Juda, R.L. Kelley, D. McCammon, C.K. Stahle, A.E. Szymkowiak, and J. Zhang, ESA Symposium on Photon Detectors for Space Instrumentation, ESA, 1992, Vol. SP-356.
[7] N. Rando, A. Peacock, C. Foden, A. van Dordrecht, J. Lumley, and C. Pereira, J. Appl. Phys. **73**, 5098 (1993).
[8] S.B. Kaplan, J. Low Temp. Phys. **37**, 343 (1979).
[9] B.L. Henke, P. Lee, T.J. Tanaka, R.L. Shimabukuro, and B.K. Fujikawa, Atomic Data & Nucl. Data Tables **27**, 1-144 (1982).
[10] W.A. Little, Can. J. Phys. **37**, 334 (1959).
[11] L.M. Brekhovskikh, *Waves in Layered Media* (Academic, New York, 1960).
[12] Y.B. Levinson, Nonequilibrium Phonons in Nonmetallic Crystals, edited by W. Eisenmenger & A.A. Kaplyanskii (1986), Vol. 16, p. 91.
[13] D.P. Singh and Y.P. Joshi, Phys. Rev. B **19**, 3133 (1979).
[14] A. Poelaert, C. Erd, A. Peacock, N. Rando, P. Verhoeve, A.G. Kozorezov, and J.K. Wigmore (unpublished).
[15] S.R. Elliott, Physics of Amorphous Materials, 2nd ed. (1990), pp. 234–242.
[16] P.W. Anderson, B.I. Halperin, and C.M. Varma, Philos. Mag. **25**, 1 (1972).
[17] W.A. Phillips, J. Low Temp. Phys. **7**, 351 (1972).
[18] W. Dietsche and H. Kinder, Phys. Rev. L. **43**, 1413 (1979).
[19] R. Orbach, Philos. Mag. B **65**, 289 (1992).